Transition from the Unipolar Region to the Sector Zone: Voyager 2, 2013 and 2014

Citation: Burlaga, L. F. et al. "Transition from the Unipolar Region to the Sector Zone: Voyager 2, 2013 and 2014." The Astrophysical Journal 841, 1 (May 2017): 47 © 2017 The American Astronomical Society

As Published: http://dx.doi.org/10.3847/1538-4357/aa6f5c

Publisher: IOP Publishing

Persistent URL: http://hdl.handle.net/1721.1/111994

Version: Final published version: final published article, as it appeared in a journal, conference proceedings, or other formally published context

The Astrophysical Journal, 841:47 (13pp), 2017 May 20 https://doi.org/10.3847/1538-4357/aa6f5c

Transition from the Unipolar Region to the Sector Zone: *Voyager 2*, 2013 and 2014

L. F. Burlaga[1], N. F. Ness[2], and J. D. Richardson[3]
[1] NASA Goddard Space Flight Center, Code 673, Greenbelt, MD 20771, USA; lburlagahsp@verizon.net
[2] Dept. of Physics and Astronomy, University of Delaware, Newark, DE 19716, USA
[3] Kavli Center for Astrophysics and Space Science, Massachusetts Institute of Technology, CA 02139, USA
Received 2017 March 23; revised 2017 April 21; accepted 2017 April 23; published 2017 May 23

Abstract

We discuss magnetic field and plasma observations of the heliosheath made by *Voyager 2* (*V2*) during 2013 and 2014 near solar maximum. A transition from a unipolar region to a sector zone was observed in the azimuthal angle λ between ~2012.45 and 2013.82. The distribution of λ was strongly singly peaked at 270° in the unipolar region and double peaked in the sector zone. The δ-distribution was strongly peaked in the unipolar region and very broad in the sector zone. The distribution of daily averages of the magnetic field strength B was Gaussian in the unipolar region and lognormal in the sector zone. The correlation function of B was exponential with an e-folding time of ~5 days in both regions. The distribution of hourly increments of B was a Tsallis distribution with nonextensivity parameter $q = 1.7 \pm 0.04$ in the unipolar region and $q = 1.44 \pm 0.12$ in the sector zone. The CR–B relationship qualitatively describes the 2013 observations, but not the 2014 observations. A 40 km s^{-1} increase in the bulk speed associated with an increase in B near 2013.5 might have been produced by the merging of streams. A "D sheet" (a broad depression in B containing a current sheet moved past *V2* from days 320 to 345, 2013. The R- and N-components of the plasma velocity changed across the current sheet.

Key words: magnetic fields – plasmas – Sun: heliosphere

1. Introduction

Voyager 2 (*V2*) crossed the termination shock (TS) at 84 au at least five times in 2007 August, moving ~30° below the solar equatorial plane (Burlaga et al. 2008; Decker et al. 2008; Gurnett & Kurth 2008; Richardson et al. 2008 and Stone et al. 2008), and it has been moving in heliosheath toward the heliopause at least through 2016. This paper discusses the observations made by *V2* from 2013.0 to 2015.0, when *V2* moved from 100.49 to 109.78 au and its latitude changed from −30.°2 S to −31.°3 S. The *Voyager* magnetic field instrument is described by Behannon et al. (1977). Key aspects of the data processing in recent years are discussed by Berdichevsky (2009, 2015). The plasma instrument on *V2* is described by Bridge et al. (1977).

During this time, solar activity increased toward its maximum level in 2014. Since the solar wind leaving the Sun during 2014 arrived at *V2* approximately a year later, *V2* was observing the solar wind in the heliosheath when solar activity was near maximum. As solar activity increases, the latitudinal extent of the heliospheric current sheet (HCS) increases (Shultz 1973). The aim of this paper is to study the magnetic field observed by *V2* in the heliosheath at 107 au ±2 au and at 31.°2 S near solar maximum conditions, when the maximal latitudinal extent of the HCS moved poleward and crossed the latitude of *V2*. We compare the transition from the sector zone to the unipolar region observed by *V2* from 2007.7 to 2009.5 with the transition from the unipolar region to the sector zone during 2013 and 2014.

2. Heliosheath Magnetic Fields Observed by *V2*

2.1. Overview

In order to place our new results in perspective, we show the observations made by *V2* in the heliosheath from 2007.0 to 2015.0 in Figure 1, which shows daily averages of the magnetic field strength B, the azimuthal angle λ, and the elevation angle δ in the spacecraft centered RTN coordinate system. The *V2* magnetic field observations from 2007.0 through 2012 have been discussed in previous papers (Burlaga et al. 2009, 2010; Richardson & Burlaga 2013). Figure 1 also includes the new observations for the years 2013 and 2014, which are the main subject of the present paper. The magnetic field strength B decreased from the time it reached the TS until the middle of 2010. A tendency for B to decrease is expected, since the solar wind is initially expanding radially as *V2* moved through the heliosheath. However, after mid-2010, there was a tendency for B to increase, which cannot be explained by a stationary flow.

As shown by Pogorelov et al. (2009) and Burlaga et al. (2009), it is essential to consider solar cycle variations when analyzing magnetic fields in the heliosheath. Solar activity was decreasing toward a minimum in 2007 when *V2* crossed the TS during 2007 (https://en.wikipedia.org/wiki/Solar_cycle). The magnetic field at 1 au reached the minimum value of 4 nT in mid-2009, which was associated with a historically low minimum of solar activity (McDonald et al. 2010; Ahluwalia & Ygbuhay 2011; Ahluwalia & Jackiewicz 2012; McComas et al. 2013). Solar activity during solar cycle 23 decreased to a minimum value in 2009 August, when the monthly mean sunspot number was zero. The sunspot number began increasing significantly in 2010 and 2011. Burlaga et al. (2014) found that the minimum latitudinal extent of the HCS from the solar equatorial plane occurred near solar minimum, at which time *V2* was in a unipolar region sampling magnetic fields from the southern coronal hole during 2011, consistent with the propagation time of the solar wind from 1 to ≈90 au being approximately 1 year. The smooth sunspot number reached a local maximum of 66.9 in 2012 February and a maximum in 2014 (making it the smallest sunspot cycle since cycle 14 in 1906) and it decreased during 2015 and 2016. Reversals of the global solar magnetic field occur within a year of solar maximum and can occur at different times in the Northern and Southern Hemisphere. In the current solar cycle

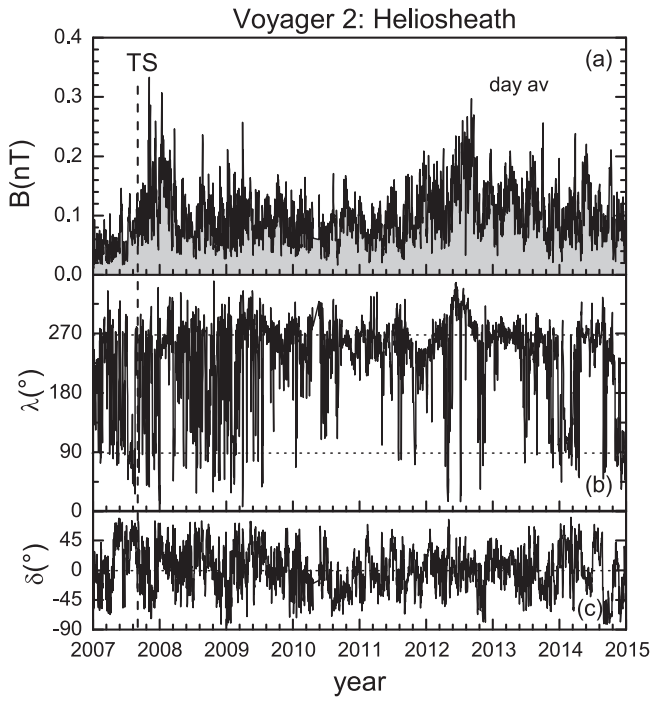

Figure 1. Daily averages of (a) the magnetic field strength $\boldsymbol{B}$, (b) azimuthal angle λ, and (c) elevation angle δ observed by *Voyager 2* from 2007 to 2015. *Voyager 2* was in the heliosheath following the termination shock, indicated by the vertical dashed line.

24 the flip from positive (away) polarity to negative (toward) polarity occurred in the southern hemisphere during 2013 July, and the change from negative to positive polarity occurred in the northern hemisphere in 2012 June.

It is well-known that when solar activity increases, the number of CMEs and magnetic clouds carrying relatively strong magnetic fields from the Sun increases, which results in an increasing average B at 1 au. As the solar wind propagates outward from the Sun and into the heliosheath, the relatively strong magnetic fields persist. Since the time for the solar wind to propagate from 1 to 100 au is approximately one year, and since B tends to vary with the sunspot number, we expect that a spacecraft in the heliosheath would observe (1) solar minimum conditions and weak magnetic fields in the heliosheath during 2010, (2) increasing solar activity and increasingly strong magnetic fields during 2011 and 2012, (3) maximum activity and strong magnetic fields in 2015, and (4) decreasing activity and magnetic field strength in the heliosheath during 2016 and 2017. Figure 1 shows that *V2* did observe minimum magnetic field strengths in the heliosheath in mid-2010 and increasing B during 2011 and 2012. A global merged interaction region (GMIR; Burlaga 1995) was observed during 2012, which produced exceptionally large magnetic fields (Burlaga et al. 2016). Relatively strong magnetic fields were also observed during 2013 and 2014, as shown in Figure 1(a), as expected from solar cycle variations.

2.2. Transition from the Sector Zone to the Unipolar Region During 2007 and 2010

In the hypothetical case in which the HCS is a constant 2D surface that always moves poleward as solar activity increases from solar minimum, there would be a well-defined transition from a unipolar region to the sector zone. Since the shape of the HCS is complex and varying as a result of waves on its surface and possibly of instability leading to fragmentation, the thickness is non-zero, the structure may be very complicated, and the motion of the current sheet is clearly non-uniform and not necessarily always one direction. Therefore, we cannot identify a simple boundary between the sector zone and the unipolar region in the observations. Nevertheless, Figure 1 shows that there is a broad interval, with no sharp boundaries (for the reasons given above) in which the magnetic field is directed primarily away from the Sun (the unipolar region) from ∼2009.6 to ∼2013.8245. Earlier, Burlaga et al. (2009, 2010), based on a limited data set, estimated that V2 was in this unipolar region from ∼2009.5 to at least 2010.3.

Prior to entering the unipolar region, V2 was in the sector zone containing magnetic fields directed alternately toward the Sun and away from the Sun. Burlaga et al. (2009, 2010) showed that the transition from the sector zone to the unipolar region was caused by the decreasing latitudinal extent of the sector zone. This motion was inferred by Burlaga et al. (2009) from variations of the neutral line on the source surface, using the solar magnetic field data from the Wilcox Solar Observatory and the Mount Wilson Observatory data. The HCS was close to the latitude of *V2* (≈−30° S) during the interval 2007.7 to 2009.4, and *V2* sampled conditions on both sides of the HCS many times during the interval. While *V2* was in the sector zone and in a transition region from 2007.7 to 2009.4 the distribution of δ was double peaked with 22% negative polarity and 78% positive polarity, and the distribution of B was lognormal.

2.3. Transition from the Unipolar Region to the Sector Zone During 2013 and 2014

Several years later, as solar activity decreased during solar cycle 23 to a minimum in 2010, the HCS moved toward the solar equatorial plane and moved below the latitude of *V2* in the southern hemisphere in the heliosheath. Thus, a transition from the unipolar region to the sector zone, was observed by *V2* in the southern hemisphere as solar activity increased during solar cycle 27. *V2* remained in the unipolar region until ∼2013.8245, as noted above in reference to Figure 1.

Figure 2 shows daily averages of the heliosheath magnetic field observed by *V2* during 2013 and 2014. A significant new result is the observation of a relatively abrupt transition from nearly unipolar "away" magnetic fields in the southern hemisphere to a magnetic field with sectors and sector boundaries, at approximately 2013.8245 as indicated by the solid vertical line in Figure 3 separating the unipolar region from the sector zone. There are times in the unipolar region when the azimuthal angles decreased toward 90° for a brief interval. In some cases, these occur when the magnetic field strength is weak and the angles cannot be measured accurately. In other cases, the changes might be real, but the duration is not long enough to indicate the passage of a "toward" sector. It is possible that these brief transitions were caused by ripples in the HCS implying that the HCS was approaching V2, beginning near the time indicated by the vertical dashed line in Figure 2.

Historically, a "sector" (Wilcox & Ness 1965) was defined as a region near 1 au in which the magnetic field vector $\boldsymbol{B}$ is along the "spiral magnetic field direction" given by the

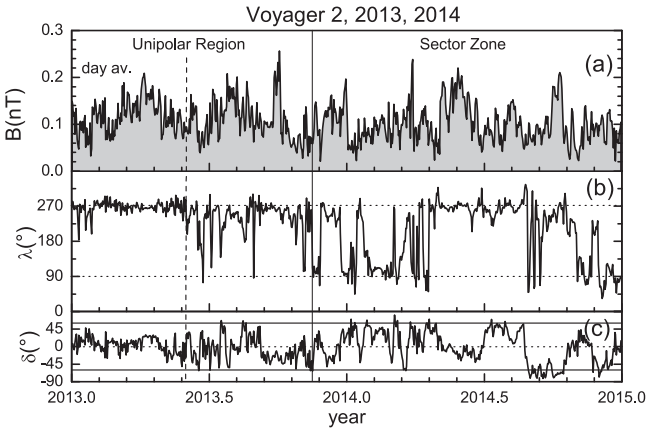

Figure 2. Daily averages of (a) the magnetic field strength $\boldsymbol{B}$, (b) azimuthal angle λ, and (c) elevation angle δ observed by *Voyager 2* from 2013.0 to 2015.0. The vertical line at 2013.8 separates the unipolar region from the sector zone. There may be a transition region in which there were large values of $|\delta|$, in which λ appears to deviate from the spiral direction 270°, though the deviations might simply represent uncertainties associated with the large elevation angles, since λ cannot be measured accurately when $|\delta|$ is large.

azimuthal angles $\lambda = 45°$ and 135° and elevation angle $\delta = 0°$ (Parker 1958, 1963) for several days or more and bounded on each side by a sector boundary (current sheet) across which $\boldsymbol{B}$ reverses sign. The sector structure is relatively well-defined and quasi-periodic during the declining phase of the cycle and more complex when it is interrupted by transients (such as CMEs including magnetic clouds) near solar maximum. The sector structure also evolves with increasing distance from the Sun, becoming more mixed and less ordered as fast flows overtake slower flows and merge with transient flows to form merged interaction regions (MIRs) and GMIRs (Burlaga et al. 1993). For example, Burlaga & Ness (1994) discuss *V2* observations that show how the sectors and regions with mixed polarity evolve to complicated polarity patterns near 33.6–36.2 au and how two MIRs can contain sectors of opposite polarity as well as mixed polarity, while the elevation angle δ still tends to be near 0°. Beyond ∼30 au, in the heliosphere and in the heliosheath, as well as in both the unipolar region and in the sector zone, *V1* observed that on average $\lambda = 90°$ and 270° and elevation angle $\delta = 0°$. In the heliosheath the sector polarity pattern became very complicated. Prior to crossing the TS, it seems from Figure 1 that at *V2* the sector structure appears to be very complex, but this is largely because it becomes more difficult to measure the angles accurately when B is relatively weak. In the heliosheath, sectors are more easily identified, because B is generally relatively strong there. For example, Figure 2(b) shows that during 2013 a sector structure is seen in $\lambda(t)$, which generally alternates between 90° and 270°, but there are a number of times when λ is not close to the spiral field direction. These deviations are discussed in more detail in Section 4.

At the beginning of 2013, *V2* was still in the unipolar region, where $\lambda = 270°$ and the average elevation angle δ was relatively close to 0°. However, careful examination of the data in Figure 2(c) indicates that relatively large deviations of δ from 0° began to appear in the heliosheath after ∼2013.4, even while *V2* was still within the unipolar zone. Large fluctuations in δ away from 0° were often observed throughout most of the sector zone, as shown in Figure 2(c). The cause of these large fluctuations is not known (except when B was too weak ($\lesssim$0.05 nT) to measure angles accurately). One possibility is that the large deviations of δ from 0° were caused by MIRs associated with the increasing solar activity. Another possibility is that magnetic reconnection becomes important in the heliosheath, where the solar wind slows down (Drake et al. 2010, 2017; Opher et al. 2011). For example, Richardson et al. (2016) found that the predicted and observed values of the sector polarity agree well in the heliosphere and heliosheath until 2012, except for in 2008 and 2009, indicating that magnetic reconnection might have been occurring in the heliosheath during those years. However, direct evidence for ongoing magnetic reconnection in the heliosheath has not yet been found.

Distributions of the angles λ and δ in the unipolar region and in the sector zone are shown in Figure 3. The λ-distribution in the unipolar region, shown in Figure 3(a), has a very pronounced peak at 270°, and no secondary peak. In contrast, the λ-distribution in the sector zone has a distinct double-peak structure, with the primary peak at $\lambda = 270°$ and the secondary peak at $\lambda = 90°$. These angles are the same as the azimuthal component of the "Parker-spiral" magnetic fields (Parker 1958, 1963) observed in the heliosphere and throughout the regions of the heliosheath explored to date. The corresponding distributions of the elevation angle δ in the unipolar region and in the sector zone are shown in Figure 3(c)) and Figure 3(d), respectively. The δ-distribution in the unipolar region was strongly peaked, with a maximum near the Parker-spiral field direction $\delta = 0°$, and with $-70° \leqslant \delta \leqslant 70°$. In contrast, the distribution of δ in the sector region was very broad, with no single strong peak.

The distributions of daily averages of B in the unipolar region and in the sector zone are plotted in Figures 4(a) and (b), respectively. The distribution of B in the unipolar region is described by a Gaussian distribution shown in Figure 4(a), which is given by the expression

$$B = B_o + (A/(w \times \sqrt{(\pi/2)})) \times \exp(-2 \times ((B - \langle B \rangle)/w)^2 \quad (1)$$

with coefficient of determination $R^2 = 0.93$. The corresponding dashed curves are the 95% confidence bands based on a t-test. The parameters derived from the fit to the Gaussian are $B_o = (0.108 \pm 0.003)$ nT, $w = (0.085 \pm 0.006) = 2\sigma$, and $A = 6.4 \pm 0.04$. The distribution of B in the sector zone shown in Figure 4(b) is a lognormal distribution of B, which is given accurately ($R^2 = 0.988$) by the expression

$$B = A'/(\sqrt{(2\pi)} \times w' \times B) \times \exp(-(\ln(B/B_c))^2/(2w'^2)) \quad (2)$$

with $B_c' = (0.090 \pm 0.002)$ nT, $w' = (0.46 \pm 0.02)$, and $A' = 8.37 \pm 0.23$.

2.4. Correlation Function of B

The autocorrelation of daily averages of B with timescale τ is described by the correlation function

$$C(\tau) \equiv \langle [B(t_i + \tau) - \langle B(t_i) \rangle] \times [B(t_i) - \langle B(t_i) \rangle)] \rangle / \langle [(B(t_i) - \langle B(t_i) \rangle]^2 \rangle \quad (3)$$

for both the unipolar region and the sector region. Linear interpolation was used to fill the few data gaps. This correlation function computed from the observations made in the unipolar

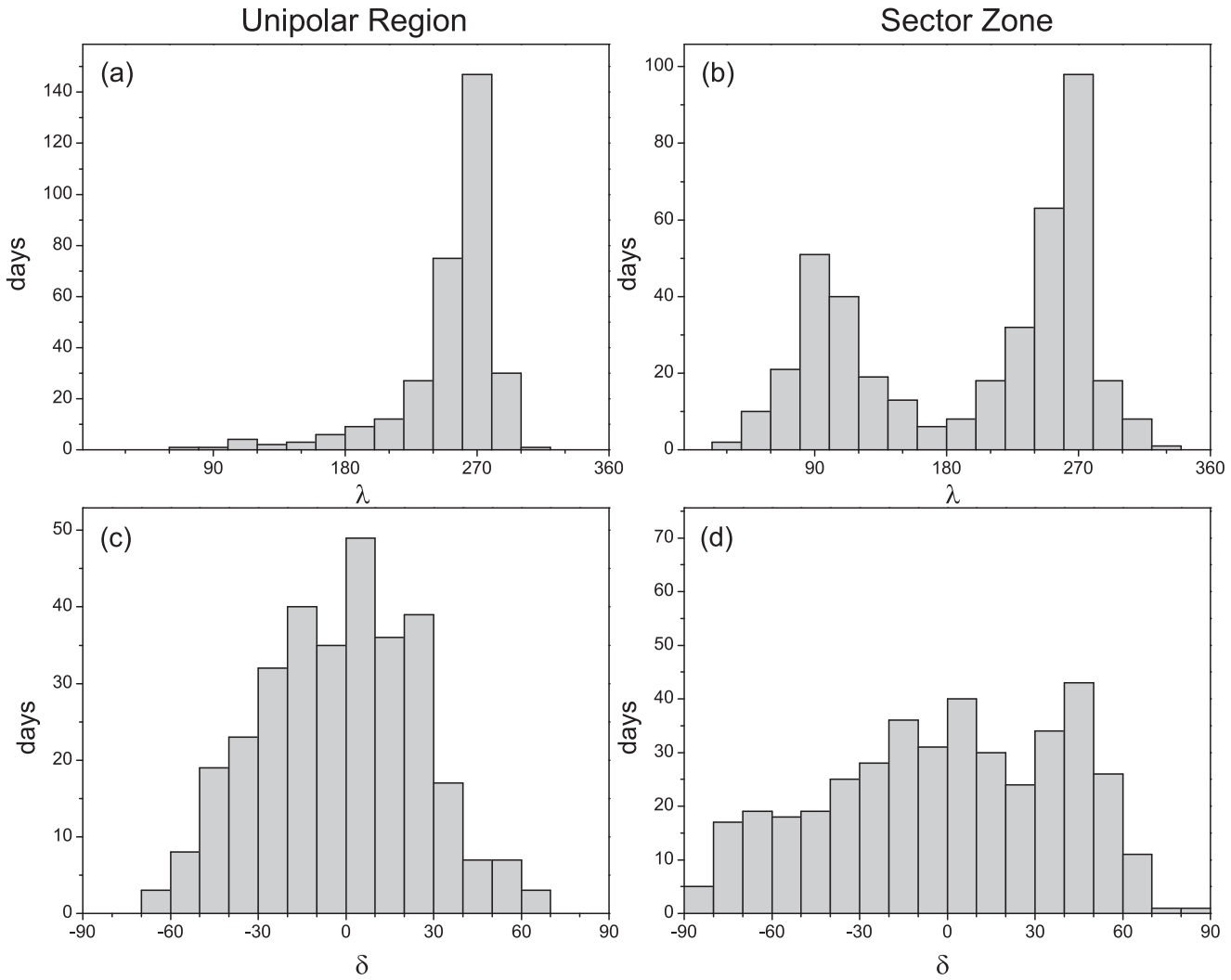

Figure 3. Distributions of λ in the unipolar region (a) and the sector zone (b) as well as the distributions of δ in the unipolar region (c) and the sector zone (d).

region and sector region are shown in Figures 5(a) and (b), respectively. In both cases, the variation of the correlation function with the scale is described by an exponential decay, $C(\tau) = A \times \exp(-\tau/\tau_e)$, as shown by the curves in the figures. The e-folding time, τ_e, is similar in both cases, namely $\tau_e = (5.3 \pm 0.06)$ days in the unipolar region and $\tau_e = (4.9 \pm 2)$ days in the sector zone. In both cases, very little correlation was observed after 16 days.

2.5. Incremental Fluctuations of B

The incremental change of B on a scale of one hour as a function of time is defined by $dB1(t) = B(t + 1\ \mathrm{hr}) - B(t))$. In many cases, one cannot measure the desired increments of hour averages, owing to data gaps, in which case, we use only the subset of increments that can be measured. There are sufficient numbers of these increments to plot meaningful distribution functions.

In the unipolar region from 2013.0 to 2013.838, measurements obtained by *V2* give the time series $dB1(t)$ that is plotted in Figure 6(a). Note the bursty, intermittent nature of the fluctuations of $dB1$, which is a signature of turbulence. In the sector region, from 2013.8245 to 2015.0, the time series $dB1(t)$ is given by the curve in Figure 7(a). A visual comparison of the time series in Figure 6(a) with that in Figure 7(a) suggests that the fluctuations of $dB1(t)$ are greater in the unipolar region than in the sector zone. In other words, the unipolar region is more intermittent than the sector zone.

Previous quantitative studies of fluctuations of increments of B over a wide range of scales in both the solar wind and in the heliosheath have shown that the measured distributions of the increments $dBn(t_i; \tau_n) = B\ (t + \tau_n) - B\ (t)$, can be described by the "Tsallis distribution"

$$A_q \times \exp_q[-\beta_q (dBn)^2] \equiv A_q [1 + (q - 1)\beta_q \times (dBn)^2]^{-1/(q-1)}. \quad (4)$$

The Tsallis distribution function has been found to describe the increments of B over a wide range of scales from 48 s to several days throughout the regions of the heliosheath observed by *V1* and *V2* (Burlaga et al. 2006, 2007; Burlaga & Ness 2013). Thus, the Tsallis distribution seems to be a nearly universal property of the solar wind and heliosheath. The Tsallis distribution of dBn is generally (but not always) associated with the multifractal structure of B observed in the heliosheath and supersonic solar wind.

The Tsallis distribution is a symmetric distribution that has a Gaussian core and power-law tails. The parameter q is the

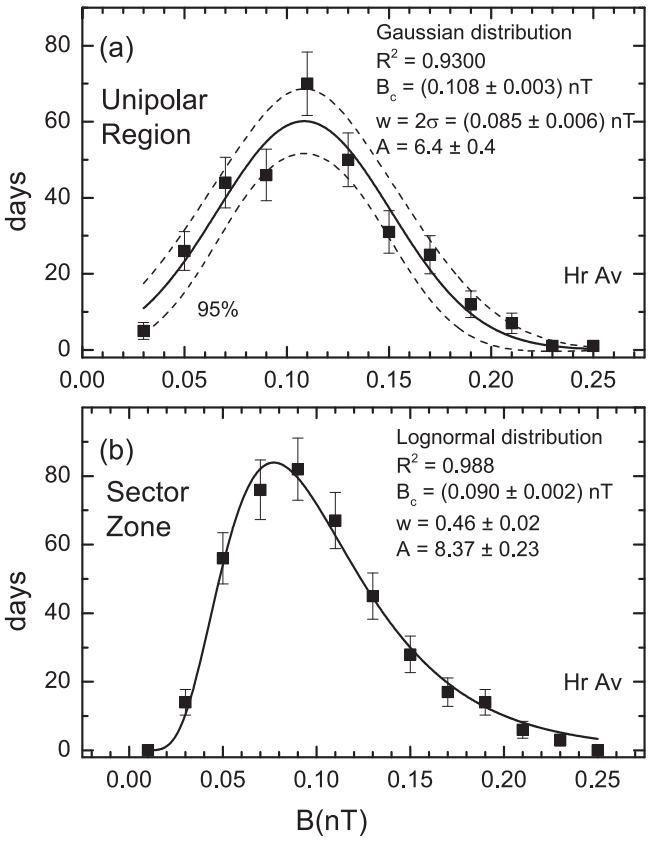

Figure 4. Distribution of B (a) in the unipolar region was a Gaussian distribution, and the distribution of (b) in the sector zone was a lognormal distribution.

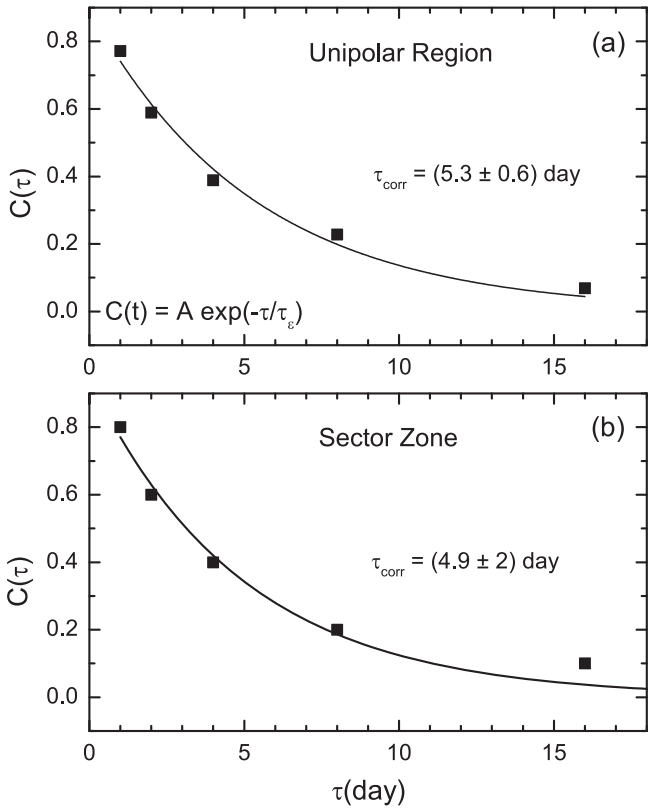

Figure 5. Autocorrelation of $C(\tau)$ of B was exponential in (a) the unipolar region and (b) the sector zone, with any folding time approximately 5 days in both cases.

"entropic index" or "nonextensivity" factor, $-\infty < q \leqslant 3$, which depends on scale (Tsallis 1988, 2009); A_q and B_q refer to Tsallis distributions with a particular q; they too depend on scale as indicated by the subscripts. In the limit $q \rightarrow 1$, the Tsallis distribution is a Gaussian distribution. Thus, we may regard $q > 1$ as a measure of the deviation from a Gaussian distribution. The parameter β is related to the width of the core of the distribution, which may be described by $w_c = \beta^{-1/2}$.

In the unipolar region, the distribution function of the measured values of hour increments $dB1$ is plotted by the points in Figure 6(b). We fit the observed PDF with the Tsallis distribution, and obtained the solid curve in Figure 6(b), which provides an excellent fit ($R^2 = 0.998$) to the observed distribution. The parameters from this fit are, $\beta = 7500 \pm 300$ and $\delta = 775 \pm 8$ and $q = 1.7 \pm 0.04$. Values of $q \sim 1.7$, which imply a significant intermittency, have often been found in distributions of hour averages of B during the intervals from several months to a year in the solar wind and the heliosheath.

In the sector region, the distribution of hour averages of $dB1$ is also very accurately described by the Tsallis distribution ($R^2 = 0.9997$), as shown by the curve in Figure 7(b). The parameters of this fit are $q = 1.44 \pm 0.12$, $\beta = 10{,}470 \pm 180$, and $A = 1286 \pm 5$. This value of q in the sector zone is less than that in the unipolar region discussed in the preceding paragraph. Since we observe $q = 1.7 \pm 0.04$ in the unipolar region and $q = 1.44 \pm 0.12$ and the sector region, the fluctuations of B were less intermittent in the sector region than in the unipolar region at the 1σ level, but we cannot definitively say that, in general, the fluctuations of B in the

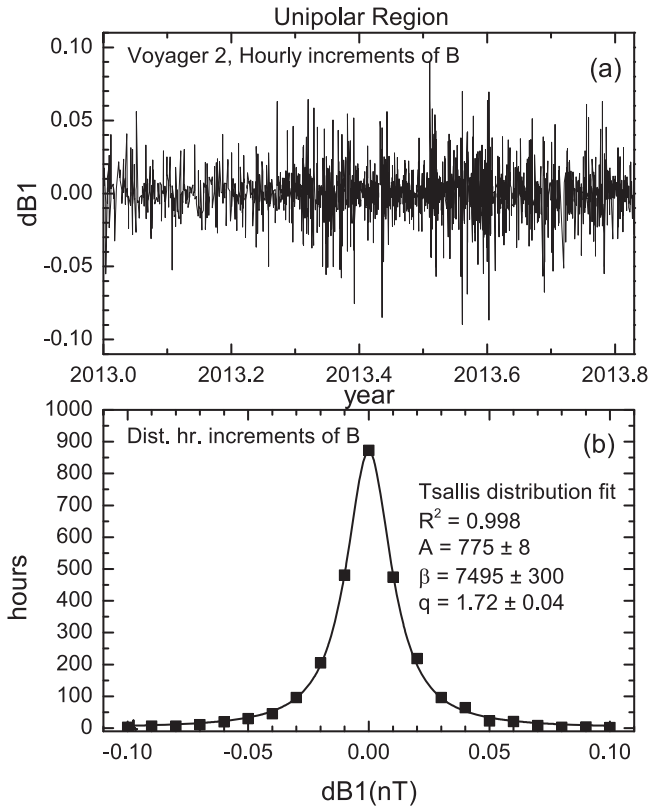

Figure 6. In the unipolar region (a), the fluctuations of hourly increments of B in the time series as a function of time are intermittent and (b) the distribution of these increments, shown by the points, is described by the Tsallis distribution with $q = 1.72 \pm 0.04$.

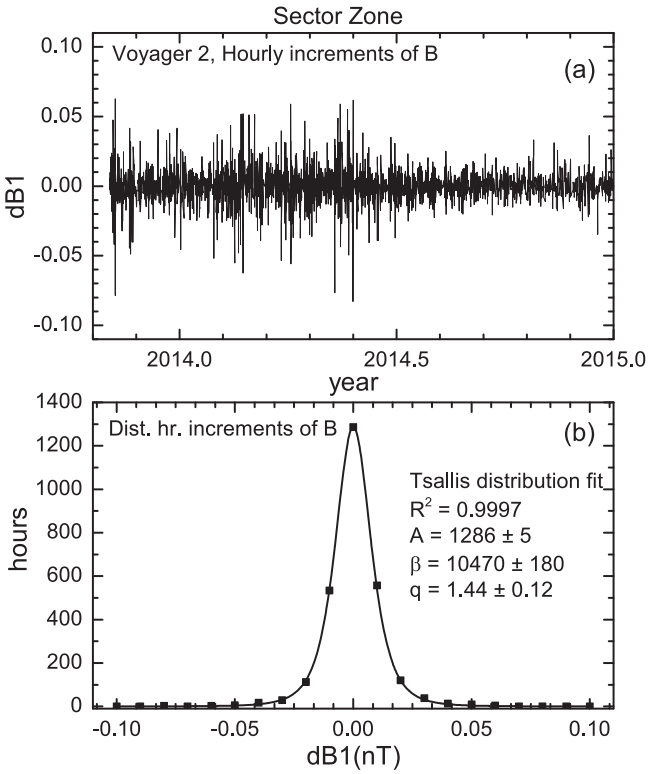

Figure 7. In the sector zone (a), the fluctuations of the hourly increments of B as a function of time are intermittent and (b) the distribution of these increments, shown by the points, is described by the Tsallis distribution with $q = 1.44 \pm 0.12$.

sector region are less intermittent than those in the unipolar region.

The variations of daily averages of $q(n)$ and $\beta(n)$ with increasing scale n in the unipolar region and sector region are shown in Figure 8. The values of $q(n)$ for n-day increments of B, where $n = 1$, 2, 3, and 4 days, are shown for the unipolar region and sector zone in Figures 8(a) and (c).

In the unipolar region, the values of daily averages of $q(n)$ calculated from fits of the Tsallis distribution to the corresponding distributions of dBn are plotted as points in Figure 8(a), and these points are accurately described by the sigmoid distribution $q(n) = q2 + (q1 - q2)/(1 + \exp((n - n_o)/w))$. This distribution passes through all of the observed values of q, though the error bars are relatively large. From this fit, we find that the value of q at a scale of one day is $q(1) = 1.38$ in the unipolar region (which is smaller than the value $q = 1.71$ derived earlier from the fit to the distribution of hour increments of B, as expected because daily averages smooth the data more than hour averages, making the fluctuations appear less intermittent. On a scale of 16 days, $q(16) = 0.96$, which is consistent with a Gaussian distribution. Thus, in the unipolar region, q decreased monotonically from 1.38 to $\sim$1 with increasing scale, and the distribution of increments of B is approximately Gaussian on scales $\gtrsim$10 days.

In the sector region, the variation of q with increasing timescale is more complicated, as shown in Figure 8(c). In this case, there is more scatter of the points, and one cannot fit the observations with a sigmoid distribution. However, a linear fit to the values of q derived from the distributions of dBn shows that there appears to be a trend for q to decrease slightly from $q(1) \sim 1.3$ for $n = 1$ to $q(16) \sim 1.1$ for $n = 16$, although the error bars are quite large. In other words, q tends to decrease with increasing n in both the sector region and the unipolar region, but the variability and uncertainty is much larger in the sector region.

As discussed in Section 2, near the end of solar cycle 26 (when *V2* was close to the TS) $q = 1.01 \pm 0.29$ in the unipolar region and $q = 1.66 \pm 0.01$ in the sector zone, whereas we found $q \sim 1.4$ in the unipolar region and $q \sim 1.3$ in the sector zone far from the TS (with large uncertainties in both cases). The reason for this difference is not known, but the evolution of the fluctuations with increasing distance in the sheath and solar activity might be an important factor to consider. In any case, there is no theory or model for the evolution of the Tsallis distribution with increasing distance in the heliosheath.

The variation of β derived from fits of the distributions of dBn to a Tsallis distribution with increasing values of n is similar for the unipolar region and the sector region, as shown in Figures 8(b) and (d), respectively. Both sets of observations are described by an exponential decay. However, the exponential decay time in the unipolar region is longer ($\sim$2.8 days) than that in the sector region ($\sim$1.3 days). In both cases, the values of β approach an "equilibrium value" $q = 1$, corresponding to Gaussian distribution, on a scale of $\sim$10 days.

3. *V2* Observations of the Magnetic Fields, Plasmas, and Cosmic Rays

3.1. The Relationship between B and the Plasma During 2013 and 2014

The relationships among daily averages of the magnetic field strength (B), density (N), temperature (T), and speed (V) of the plasma in the heliosheath during 2013 and 2014 are shown in Figure 9. Inspection of this figure shows that, as usually observed in the heliosheath, B, N, and T are not strongly correlated. This is because the pressure of the plasma is dominated by particles with energies greater than those measured by the solar wind experiment on *V2,* (e.g., Krimigis et al. 2010). Nevertheless, there is one particularly interesting feature, labeled A in Figure 9, namely a relatively large increase in the bulk speed, from $\sim$140 to 180 km s^{-1}, related to the increasing B. Burlaga et al. (2005) showed that a similar increase in the speed measured by *V2* near 70 au was produced by the merging of a sequence of increasingly fast corotating streams within approximately 10 au from the Sun. That paper also models this merging process and its evolution out to 70 au, which shows the formation and growth of a MIR, that becomes relatively weak at 70 au. It would be interesting to determine whether this event or some other event during the same year could have produced the *V2* observations shown in Figure 9. We leave this problem to others who have MHD codes capable of following the evolution of the flows and magnetic fields through the heliosphere, across the TS, and within the heliosheath. The basic evolution is governed by the momentum flux out to the distant heliosphere, but it will be necessary to consider the effect of the TS, as well as the tendency of the flow to diverge in latitude and longitude the heliosheath as a consequence of the interaction with the interstellar medium.

3.2. Magnetic Flux Deficit?

For a radial flow in the heliosheath and solar wind, the magnetic flux BVR and the solar wind and heliosheath versus time (hence distance) is expected to be a conserved quantity

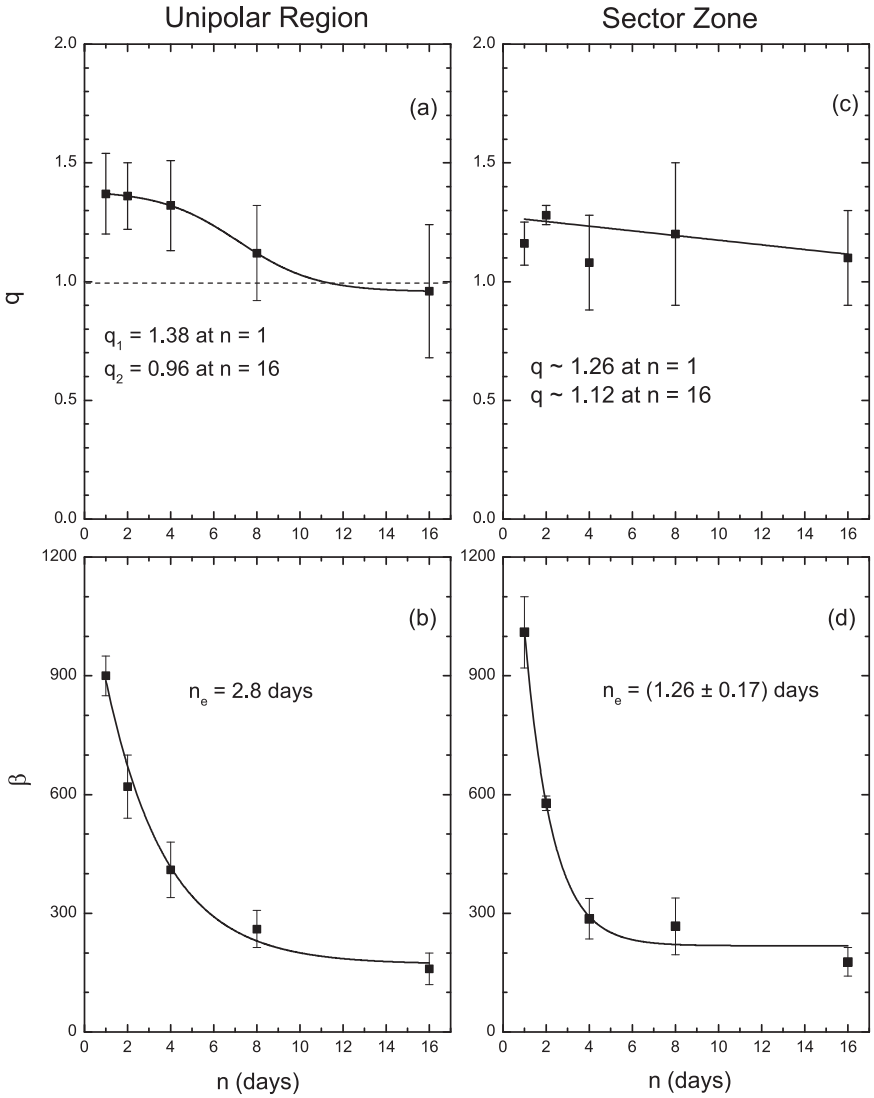

Figure 8. Nonextensivity parameter q derived from the distribution function of n-day increments of B decreases with increasing n (a) significantly in the unipolar region from $q = 1.4$ for increments of 1 day to 1.0 for increments of 16 days and (c) less clearly in the sector zone from $q \sim 1.26$ for increments of 1 day to $q \sim 1.1$ for increments of 16 days. The width parameter β decreased exponentially with increasing time in both (b) the unipolar zone and (d) the sector zone.

(Parker 1958). However, a plot of this versus time (distance) using *V1* observations in the heliosheath shows that this quantity is not conserved (Richardson et al. 2013) in the heliosheath. It has been suggested that this result is a consequence of a significant decrease in the magnetic field strength caused by magnetic reconnection (e.g., Drake et al. 2010, 2017; Opher et al. 2011). Of course, the observed decrease in BV_RR could have been produced by a decrease in V_R alone. On the other hand, the *V2* observations show that BV_RR is nearly conserved in the region of the heliosheath that has been observed to date because there has been neither a large decrease in V_R nor a large decrease in B (Richardson et al. 2013). Richardson et al. (2016) have identified a few years when magnetic reconnection might be present in the *Voyager* observations, associated with fewer sector boundaries than predicted by extrapolations from the Sun. Figure 10 shows that the magnetic flux continued to be approximately conserved as seen by *V2* through 2013 and 2014, though there was a slight tendency for the flux to decrease with increasing time. This tendency might be a consequence of the component of the flow directed away from the radial direction and therefore carrying magnetic flux away from the nose direction. However, it is conceivable that part of this small decrease in the magnetic flux is a consequence of magnetic reconnection.

3.3. CR–B Relationship

An empirical qualitative relationship between B and the cosmic-ray intensity (CRI) profile (the "CR–B relationship") has been observed and modeled empirically by two parameters by Burlaga et al. (1985, 2005) for both *V1* and *V2* observations from 10 to ~120 au. Basically, the relationship says that if B is greater than average during a single year, then the cosmic-ray flux tends to decrease (at a rate proportional to B), and when B is less than the average the cosmic-ray counting rate tends to increase (at a constant rate). Thus, near solar minimum, when there are a few ejecta carrying strong magnetic fields away from the Sun, the cosmic-ray counting rate increases. Near solar maximum, when one occasionally sees very strong magnetic fields for two or three solar rotations, a net decrease in the cosmic-ray counting rate during the solar cycle is observed. The average value of B in the unipolar region was

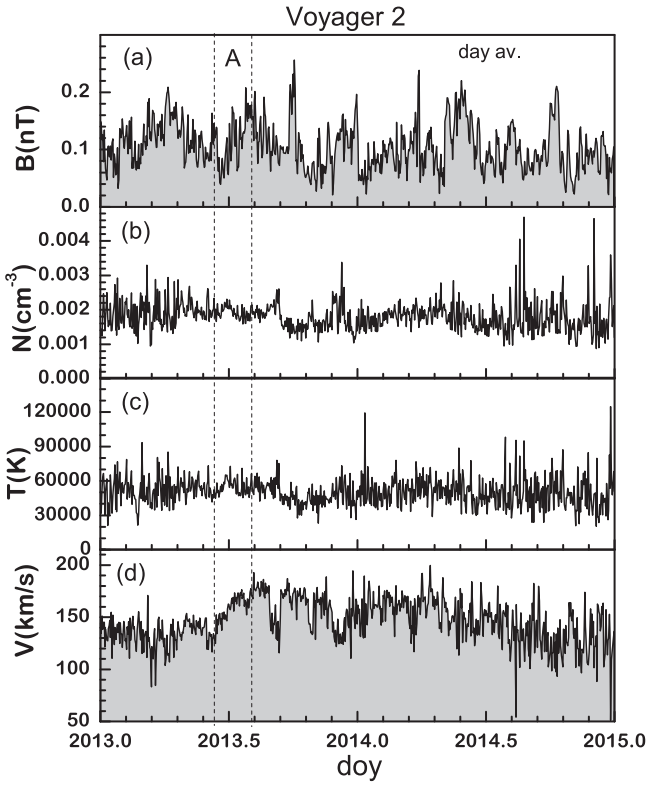

Figure 9. *Voyager 2* observations of daily averages of (a) the magnetic field strength, (b) the density, (c) proton temperature, and (d) the bulk speed of the plasma.

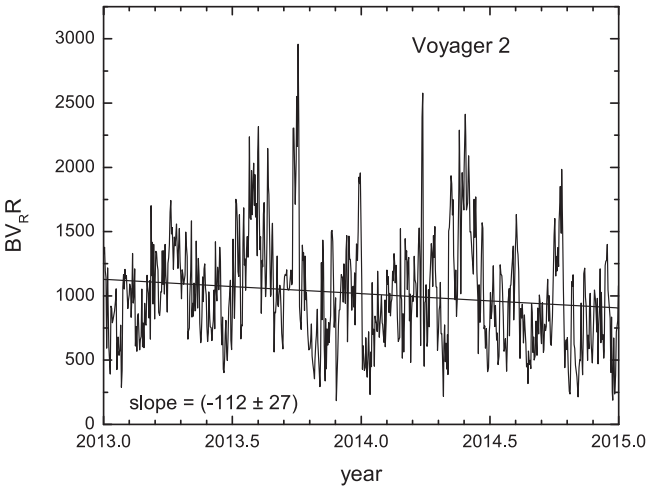

Figure 10. Magnetic flux as a function of time from 2013.0 to 2015.0. The linear fit shows only a small tendency for the magnetic flux to decrease with increasing time and distance.

(0.112 ± 0.003) nT, and that in the region with sectors was somewhat lower, (0.090 ± 0.002) nT. Figures 11(a) and (b) show B and the counting rate of cosmic rays greater than >70 MeV smoothed with a 26 day averaging filter. There were three significant depressions in the CRI during 2014 and 2015, beginning at the times of the dashed lines marked 1, 2, and 3, respectively. The first depression corresponds to a significant peak in B, which was followed by magnetic strengths less than average and a corresponding recovery of the CRI, which is qualitatively consistent with the CR–B relationship. The second major CRI decrease began with a peak in B at line 2, but there

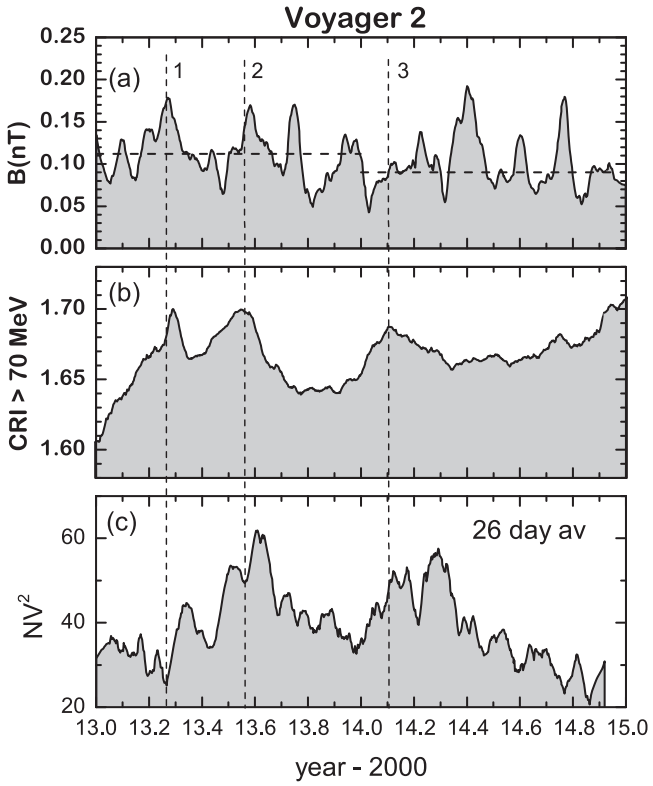

Figure 11. Twenty-six day averages of (a) the magnetic field, (b) the counting rate of the >70 MeV cosmic rays, and (c) NV^2 from 2013.0 to 2015.0. The major decreases in the cosmic-ray intensity related to both the magnetic field strength and NV^2 during the intervals 1 and 2 in 2013, but they are only related to NV^2 during 2014.

were two other peaks in B that are not consistent with the CR–B relationship. The third major decrease in CRI began at the time of line 3 with only a relatively weak increase in B, and it reached a plateau during the passage of a relatively strong enhancement in B centered at 2014.4, in contradiction to the expected decrease in CRI. A fourth (moderate) enhancement in B occurred near 2014.6 without a significant decrease in the CRI, and a final (significant) enhancement in B was accompanied by only a small reduction in the CRI. Thus, the observed profile of this cosmic rays is not qualitatively consistent with the CR–B relationship during 2014.

Each of the enhancements in CRI B in Figure 11(a) probably corresponds to an MIR (Burlaga et al. 1993, 2014) produced by the interaction of two or more ejecta or corotating interaction regions. None of the MIRs had a strong and sustained (lasting two or more solar rotations) enhancement in B, indicating that *V2* observed no GMIRs during 2013 and 2014, in contrast to the GMIR observed by *V2* during 2012 (Burlaga et al. 2016). The absence of a GMIR is consistent with the fact that there was no net decrease in the CRI from 2013 to 2014.

In general, magnetic fields and plasma observed in the heliosheath do not pass through the heliopause except when there might be significant magnetic reconnection at the heliopause. However, the enhancements in the magnetic and thermal pressure upstream of the TS can alter its speed and position, though the corresponding change in the location of the heliopause is relatively small (e.g., Washimi et al. 2011). Moreover, the MIRs and GMIRs associated with enhancements in the magnetic fields and plasma in the heliosheath can be moving fast enough to produce shocks or a pressure waves in

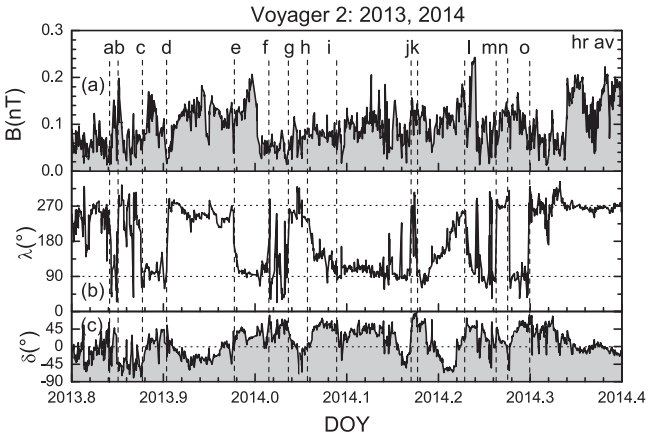

Figure 12. Sector structure observed by *Voyager 2* from 2013.8 to 2014.2 is shown by the azimuthal angle λ in panel (b) together with the elevation angle δ and (c) and the magnitude B of the magnetic field (c). The elevation angles are often unusually large, indicating that the sectors are not like those in an ideal Parker spiral field.

the heliosheath that can pass through the heliopause and into the local interstellar medium (LISM; Whang & Burlaga 1994). In particular, large changes in VN^2 can act on the heliopause and produce pressure pulses or weak shocks. Therefore, Richardson et al. (2017) calculated VN^2 observed by *V2* at times corresponding to shocks and the plasma waves observed by *V1* in the LISM (Gurnett et al. 2013, 2015). A large momentum flux associated with the GMIR observed by *V2* during 2012 (Burlaga et al. 2016) did produce the plasma wave and a shock or pressure wave observed by *V1*.

Richardson et al. (2017) also found that two of the pressure pulses observed by *V1* in the LISM were associated with (1) two large enhancements $\boldsymbol{NV}^2$ observed by *V2* during 2013 and 2014 and (2) two corresponding major long-lasting decreases in CRI. These two enhancements in $\boldsymbol{NV}^2$ are shown in Figure 11(c), which we computed using the plasma data available from http://web.mit.edu/space/www/voyager.html. Figure 11 shows that there were no large and long-lasting enhancements in B associated with the long-lasting decreases in CRI. In other words, the pressure pulses observed by *V1* were produced by two large increases in $\boldsymbol{NV}^2$, rather than by the magnetic fields in individual MIRs or GMIRs observed by *V2*.

4. Sector Structure

As discussed in Section 2, sectors and sector boundaries began to reappear in the *V2* magnetic field observations at the end of 2013, and they persisted throughout 2014. A closer look at the sectors and sector boundaries is shown in Figure 12, which is a plot of hour averages of B observed by *V2* from 2013.8 to 2014.4. It is obvious from inspection of Figure 12 that B is no longer unipolar after 2013.8. Certain "sectors" stand out in the plots of λ versus time, such as the "toward" sectors c–d, e–f, i–j, and n–o as well as the "away" sectors d–e and m–n, and the sector following "o" which extended to at least 2014.4.

On the other hand, other polarity changes are ambiguous, such as a–b, b–c, e–g, and j–k. Moreover, the azimuthal angle indicates that the intervals h–i and k–l are simply broad transitions from "away" and "toward" polarity, respectively. In order to understand the ambiguous sectors and broad transitions, one must consider two things. First, the uncertainty in the measurements of the angles depends on B, because the uncertainty in the measured components of B are large when $B < 0.05$ nT. Second, the azimuthal angle is undetermined when $\delta = 90°$, and it is highly uncertain when the absolute value of θ is greater than $\sim 65°$. Based on this criterion, we can conclude that the fluctuations of λ in the interval f–g are not real, hence e–g could be a sector. For the same reason, the broad transition from away to toward polarity in interval h–i, the narrow "sector" j–k, the broad transition k–l, and the complicated transition l–m may not be real. During the interval b–c, B was weak part of the time, which would explain the large fluctuations in the azimuthal and elevation angles during interval b–c; consequently, b–c might be a real sector that is partly obscured by the uncertainties associated with the weak B.

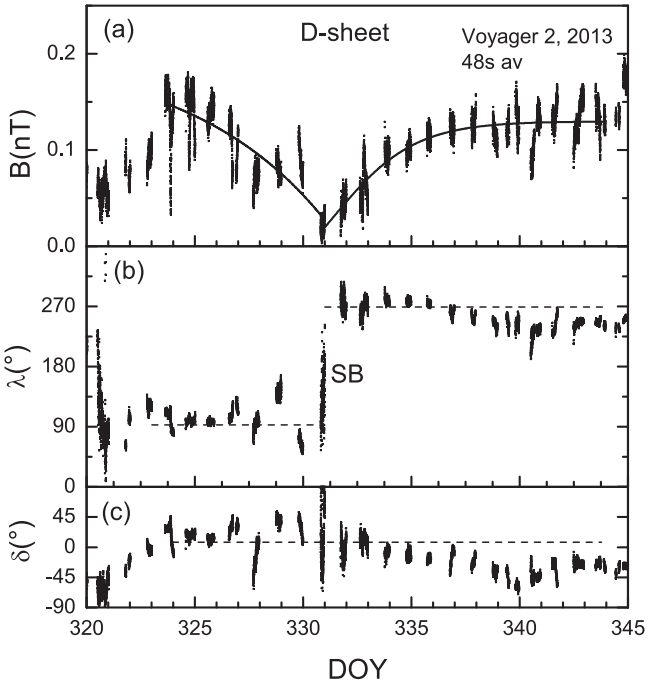

Figure 13. "D-sheet defined by (a) a broad variation of B between day 323 and day 345, 2013, and (b) a thin current sheet corresponding to a sector boundary on day 330, together with (c) the elevation angle.

We can draw two significant conclusions from these data. First, sectors were present from 2013.8 to 2014.4, which means that the HCS extended to latitudes greater than that of *V2*. Second, the sector structure was not periodic, since the "sizes" (durations) of sectors varied. It is also possible that there were ripples on the current sheet (Burlaga & Ness 1994), and we should allow for the possibility that the HCS might be patchy as a result of magnetic reconnection on theoretical grounds (Pogorelov et al. 2017).

5. An Unusual Sector Boundary: A D-sheet

Magnetic field observations of the sector boundary observed by *V2* on day 330, 2013 (shown by the vertical dashed line marked "d" in Figure 12 and are plotted at higher resolution in Figure 13). The data points in Figure 13 are 48 s averages of $\boldsymbol{B}$, and one can see that the observations were obtained only during a fraction (about a third) of each day, owing to telemetry restrictions. This sector boundary is evident in the azimuthal angle λ in Figure 13(b), which changed abruptly during day 330 from 90° to 270°. The vertical bands of observations of 48 s averages of λ and δ on day 330 are a sample of the data

within the current sheet associated with the sector boundary. This sample shows that the 48 s averages of λ changed by nearly 100° during a short time within current sheet. We can only say that the passage time of the current sheet was within the interval between the last time that λ was equal to ~90° on day 329 and the first time that λ was first observed with the angle ~270° before day 331. The elevation angle δ ranged from +90° to approximately −70° within the current sheet associated with a sector boundary (Figure 13(c)). These variations of the 48 s averages of angles are strongly affected by measurement uncertainties, so that a meaningful minimum variance analysis of this sector boundary is not possible using 48 s averages.

Figure 13 shows that B was close to zero (<0.02 nT) at the time of the sector boundary crossing. The magnetic field strength decreased from ~0.15 nT at the end of day 324 to a minimum value near 0 nT on day 330, and it then increased to ~0.13 on day 344, as shown by the solid curves in Figure 13(a). Each of the two segments of this current curve was modeled by the sigmoid function

$$B(\mathrm{t}) = B2 + (B1 - B2)/(1 + \exp((t - t_o)/w).$$

The structure of the D-sheet described in Figure 13, with a broad depression in B and a very rapid change in the magnetic field direction at the time when B was a minimum resembles the D-sheet first identified in Pioneer 10 observations by Burlaga & Ness (1968), who called them D-sheets because of the change in the direction of $\boldsymbol{B}$ and the broad decrease in B. A set of similar D-sheets, with smaller angle changes θ, in which B varied as $B_o \cos(\theta)$ led to the hypothesis that the structures might have been produced by magnetic reconnection, which would give the observed dependence on θ (Burlaga 1968). For the D-sheet in Figure 13, the angle θ is close to 180°, and the minimum B is close to zero, which suggests that the structure might have been produced by the magnetic reconnection of two oppositely directed magnetic fields. Burlaga (1968) also showed that the temperature, density, and bulk speed in a D-sheet are highest where B is lowest, which they noted is the signature of "a jet of matter squeezed out by the incoming flux tubes" as proposed by Dungey (1961). This is the signature observed by Gosling (2012) who identified magnetic reconnection in the solar wind at 1 au. Definitive observations of the reconnection observations were presented by Gosling, based on a relationship between the velocity change and a magnetic field change in each component of these vectors. However, it is possible that *V2* might have been observing either a different structure (such as a pressure balanced structure) that remained after completion of the reconnection process or a structure that formed by a process other than magnetic reconnection. The absence of the peak in the velocity at this current sheet is consistent with the observation of a static or stationary structure, rather than a structure associated with dynamic ongoing magnetic reconnection.

A minimum variance analysis of the 48 s averages of $\boldsymbol{B}$ from just before to just after the sector boundary associated with a reversal in the direction of $\boldsymbol{B}$ within the D-sheet on day 330 did not give a meaningful minimum variance direction because of the scatter of the measurements in the very weak magnetic fields (−0.03 to 0.02 nT) during the interval in which $\boldsymbol{B}$ changed sign. However, a minimum variance analysis of the hour averages of $\boldsymbol{B}$ within the sector boundary (from day 329, hour 20 to day 330, hour 24) gave the results shown in Figure 14. There was essentially no significant change or

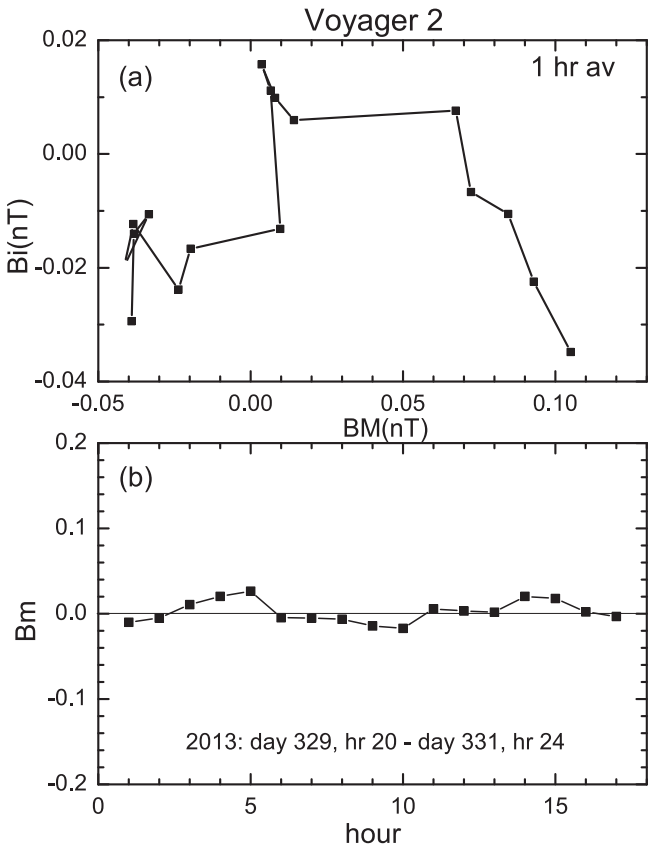

Figure 14. Panel (a) shows the rotation of two components of $\boldsymbol{B}$ in the minimum variance plane in the sector boundary shown in Figure 13, and panel (b) shows the component of $\boldsymbol{B}$ in the minimum variance direction as a function of time.

departure from zero of the component $\boldsymbol{B}(t)$ in the minimum variance direction $\boldsymbol{Bm}$ (Figure 14(b), which was determined to be $\boldsymbol{Bm} = 0.097\,\boldsymbol{R} - 0.059\,\boldsymbol{T} - 0.034\,\boldsymbol{N}$, where $\boldsymbol{R}$, $\boldsymbol{T}$, $\boldsymbol{N}$ are unit vectors in the *RTN* coordinate system. Significant rotations of the components of $\boldsymbol{B}$ in the intermediate direction ($\boldsymbol{Bi}$) and the maximum variance direction ($\boldsymbol{BM}$) were observed in the plane normal to the minimum variance direction (Figure 14(a). The minimum variance direction $\boldsymbol{Bm}$ was within 20° of the radial direction, which implies that locally the plane of the HCS was nearly orthogonal to the radial direction. The maximum variance direction $\boldsymbol{BM}$ was 28° from the tangential direction $\boldsymbol{T}$, so that $\boldsymbol{B}$ changed primarily in the $\boldsymbol{BM}$ direction.

The components of the magnetic field $\boldsymbol{B}$ = (*BR, BT, BN*) associated with the broad D-sheet discussed above are plotted from day 323 to day 338, 2013, in Figure 15. The component $BR(t)$ in Figure 15(d) was very close to 0 throughout the interval ($\langle BR\rangle = (-0.11 \pm 0.02)$ nT), and BN (t) decreased linearly from 0.05 nT on day 323 to −0.03 nT on day 338 (Figure 15(c)). However, the variation of $\boldsymbol{B}$ was primarily in the BT direction (Figure 15(b). The angle between the BT direction and the maximum variance direction $\boldsymbol{BM}$ = (0.021, 0.088, 0.422) in the *RTN* coordinate system was only 28°. The variation of the BT component from day 323 to day 338 is accurately described by the sigmoid distribution, $BT = BT_2 + (BT_1 - BT_2)/(1 + \exp((\mathrm{day} - t_o)/w))$, where $BT_1 = (0.016 \pm 0.009)$ nT, $BT_2 = (-0.132 \pm 0.009)$ nT, t_o = day 330.5 ± 0.2, and $w = 2.3 \pm 0.3$ nT. Note that $BR \sim BT \sim BN \sim 0$ when the current sheet moved past *V2*, on day 330.5 ± 0.2. Thus, to first approximation, $\boldsymbol{B}$

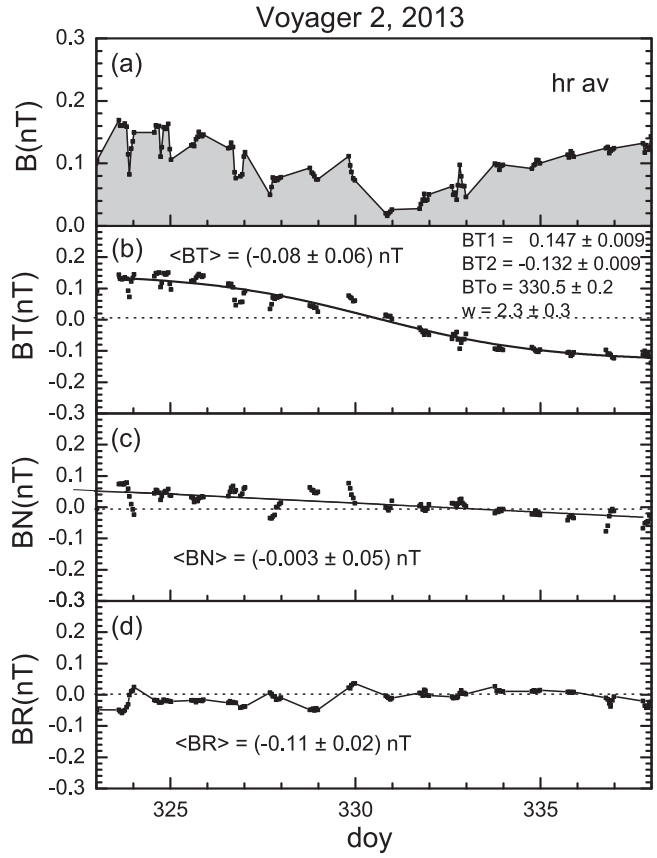

Figure 15. Magnetic field variation $\boldsymbol{B}(t)$ across the D-sheet shown in Figure 13 as a function of time from day 323 to day 335, 2013, given by (a) the magnetic field strength B, (b) the BT component of $\boldsymbol{B}$, (c) the BN component of $\boldsymbol{B}$, and (d) the BR component of $\boldsymbol{B}$ in the spacecraft centered the RTN coordinate system.

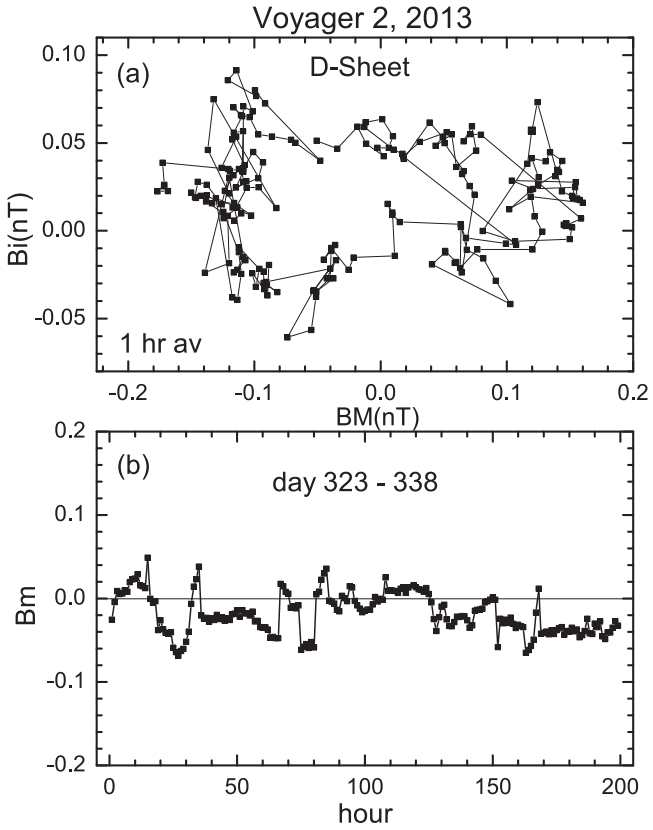

Figure 16. Panel (a) shows the rotation of two components of $\boldsymbol{B}$ in the minimum variance plane observed from day 323 to day 338, 2013, shown in Figure 13, and panel (b) shows the component of $\boldsymbol{B}$ in the minimum variance direction as a function of time.

changed primarily in one direction, and B decreased monotonically from +0.16 nT on day 323, to 0 nT on day 330.5 at the time the sector boundary was observed on day 330, and it continued to decrease with negative values until it reached −0.13 nT on day 338. In other words, from day 323 through the 338, the ∼180° change in the magnetic field direction across the sector boundary was caused primarily by the change in the sign of BT as $V2$ quickly crossed the thin current sheet. To first approximation the $\boldsymbol{BT}$ component of $\boldsymbol{B}$ varied across the D-sheet in essentially the same way that $\boldsymbol{B}$ varies transversely across a Harris current sheet, which is used in many models of magnetic reconnection.

A minimum variance analysis of the hour average components of $\boldsymbol{B}$ throughout D-sheet, from day 323 to day 338 is shown in Figure 16. The fluctuations of the component of $\boldsymbol{B}$ in the minimum variance direction $\boldsymbol{Bm}(t)$, shown in Figure 16(b) fluctuated about $Bm = 0.018$ nT, consistent with a tangential discontinuity or a weak rotational discontinuity, within the uncertainties. The component of $\boldsymbol{B}$ in the minimum variance direction (the normal to the tangential discontinuity for the current sheet) is $\boldsymbol{Bm} = 0.96\boldsymbol{R} + 0.57\boldsymbol{T} - 0.27\boldsymbol{N}$, indicating that the angle between the minimum variance direction and the radial direction $\boldsymbol{R}$ was small, ∼16°. The fluctuations of the components of $\boldsymbol{BM}$ and $\boldsymbol{Bi}$ in the minimum variance plane are shown in Figure 16(a), which shows that the large change in the direction of $\boldsymbol{B}$ between day 329 and 330 occurred by means of a rotation normal to the minimum variance direction. The maximum variance direction is primarily in the $\boldsymbol{T}$ direction, the angle between $\boldsymbol{BM}$ and $\boldsymbol{T}$ being 24°.

It is notable that there was a change in the velocity $\boldsymbol{V}$ across the relatively thin current sheet associated with the sector boundary on day 330, near the point where $B \sim 0$ nT, at which point each component of $\boldsymbol{B}$ (most prominently the $\boldsymbol{BT}$ component of $\boldsymbol{B}$) changed from positive to negative values as shown in Figure 17(e). Despite the large scatter in the components of $\boldsymbol{V}$, the sigmoid function provides good fits to the observations of these components during the intervals from day 323 to day 338. A change in direction of $\boldsymbol{V}$ was observed in the VR and VN components, which occurred across the narrow current sheet, where B was ∼0 nT. There was no significant change in either VT or BR across the current sheet on day 330. Thus, the relatively abrupt change in the direction $\boldsymbol{V}$ across the current sheet on day 330 was in the $\boldsymbol{R}$–$\boldsymbol{N}$ plane, hence perpendicular to $\boldsymbol{T}$. We conclude that the change in the direction of the velocity was directed nearly along the direction of the magnetic field discussed in the previous paragraph.

From the sigmoidal fits to the velocity components in Figure 17, we found that VR decreased from $(102.6 \pm 1.5)\,\mathrm{km\,s^{-1}}$ to $(83.7 \pm 1.9)\,\mathrm{km\,s^{-1}}$, across the sector boundary, while VN changed from $(-79.5 \pm 3.8)\,\mathrm{km\,s^{-1}}$ to $(-50.5 \pm 4.5)\,\mathrm{km\,s^{-1}}$. There was no change in VT, except for a small increase on day 324.9 which is an artifact of the fitting procedure. Thus, the change in the magnitude of the vector $\boldsymbol{V} = (VR, VT, VN)$ across the sector boundary was $(35 \pm 6)\,\mathrm{km\,s^{-1}}$, which is to be

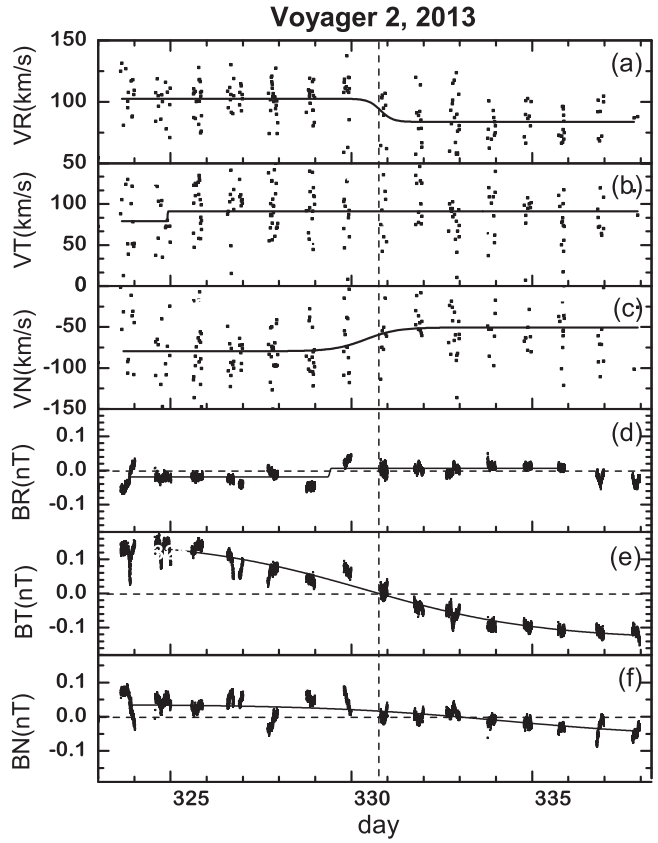

Figure 17. Components of the velocity and magnetic field across the D-sheet shown in Figure 13: (a) *VR*, (b) *VT*, (c) *VN*, (d) *BR*, (e) *BT*, and (f) *BN*.

compared with the total bulk speed $(152 \pm 5)\,\mathrm{km\,s^{-1}}$ and $(134 \pm 5)\,\mathrm{km\,s^{-1}}$ during the days before and after the sector boundary moved past *V2*, from day 323 and day 338, respectively.

The change in $\boldsymbol{V}$ ($\boldsymbol{V}'$) was a vector in the *N*–*R* plane; hence $\boldsymbol{V}'$ was perpendicular to $\boldsymbol{T}$ (and also nearly perpendicular to $\boldsymbol{B}$, which was close to $\boldsymbol{T}$-direction). The change in the $\boldsymbol{B}$ ($\boldsymbol{B}'$) was a vector nearly parallel to $\boldsymbol{T}$. Although the electric field in the solar wind frame is 0 in the MHD approximation, the perturbations $\boldsymbol{V}'$ and $\boldsymbol{B}'$ produced an electric field $\boldsymbol{E} = \boldsymbol{V}' \times \boldsymbol{B}'$, which is not equal to zero within the current sheet, and therefore capable of driving a current in the current sheet near day 330, 2013. Lemaire & Burlaga (1976) calculated the electric fields and currents required to maintain a stationary current sheet (proton boundary layer). We leave it to others to calculate whether the current obtained from our results is sufficient to drive magnetic reconnection or perhaps simply a stationary current sheet.

6. Summary

A transition "A" from a unipolar region with positive "away" magnetic polarity to the sector zone during a period of increasing sunspot number during solar cycle 24 was observed in the azimuthal angle λ in the magnetic field $\boldsymbol{B}$ observed by *V2* between ~2013.0 and 2013.8245, when *V2* was in the heliosheath. The corresponding transition "B" from the sector zone to the same unipolar region of positive magnetic polarity was observed earlier by *V2* when the sunspot number was decreasing to a minimum in solar cycle 23 from ~2007.7 to ~2009.6 after *V2* crossed the TS and entered the heliosheath. This paper discusses the magnetic field and plasma observations of the heliosheath made by (*V2*) in the unipolar region and sector zone during 2013 and 2014, when *V2* moved from 100.49 au to 109.78 near $-30\overset{\circ}{.}5$ S. The distribution of λ was strongly peaked at 270° in the unipolar region, and the distribution was double peaked at $\lambda = 90°$ and $\lambda = 270°$ in the sector zone. The δ-distribution was strongly peaked in the unipolar region; however, it was very broad in the sector zone, because the sector boundaries were often accompanied by large enhancements in $|\delta|$. Large values of $|\delta|$ are not expected in a "Parker-spiral" magnetic field. The distribution of daily averages of the magnetic field strength B was Gaussian in the unipolar region and lognormal in the sector zone, as was observed in the earlier transition "A." The autocorrelation function of B was exponential with an e-folding time of ~5 days in both regions. This function was observed to be a power law when multifractal structure was observed in the heliosheath (Burlaga & Ness 2013).

The distribution of hourly increments of B was a Tsallis distribution with nonextensivity parameter $q = 1.72 \pm 0.04$ in the unipolar region and $q = 1.44 \pm 0.12$ in the sector zone. The distribution of daily increments of B was a Tsallis distribution with $q \sim 1.38 \pm 0.15$ in the unipolar region and $\sim 1.26 \pm 0.15$ in the sector zone. The latter values are significantly different than those observed near the earlier transition "A," where $q = 1.0 \pm 0.29$ the unipolar zone and $q = 1.66 \pm 0.01$ and the sector zone. The reason for this difference is not known. However, it should be noted that the transition "A" occurred approaching solar minimum just beyond the TS, whereas the transition "B" occurred approaching solar maximum four years later and farther in the heliosheath. The radial and temporal evolution of the Tsallis distribution as a function of scale in the heliosheath would be an interesting subject for a theoretical investigation.

Qualitatively, the CR–B relationship describes the 2013 observations, but not the 2014 observations. On the other hand, the decreases in the CRI during 2013 and 2014 were associated with the passage of flows with high $\boldsymbol{NV}^2$. A $40\,\mathrm{km\,s^{-1}}$ increase in the bulk speed associated with increasing B was observed near 2013.5, which could have been produced by the merging of streams. The magnetic flux observed by *V2* during 2013 and 2014 continued to be slightly decreasing with increasing distance from the Sun, as observed previously in the heliosheath.

A "D-sheet" (a broad depression in B between containing a thin current sheet across which λ changed by 180° in several hours or days) moved past *V2* from day 320 to 345, 2013, containing a sector boundary observed on day 330. The *R*- and *N*-components (but not the *T*-component) of the plasma bulk velocity $\boldsymbol{V}$ changed significantly across the current sheet associated with the sector boundary, in a plane that was nearly perpendicular to the direction of $\boldsymbol{B}$ observed from days 320 to 345 (which was close to the direction of $\boldsymbol{T}$). The change in the velocity across the current sheet cannot be a simple shear from one side of the current sheet to the other, which would imply a change in a plane parallel to the direction of $\boldsymbol{B}$. There was a rotation of the weak magnetic field near the current sheet defining a minimum variance direction of $\boldsymbol{B}$ in this region, which was close to the radial direction $\boldsymbol{R}$, but the rotation of $\boldsymbol{V}$ was not in the minimum variance direction of $\boldsymbol{B}$.

L.F.B. was supported by NASA contract NNG14PN24P.

References

Ahluwalia, H. S., & Jackiewicz, J. 2012, AdSpR, 50, 662
Ahluwalia, H. S., & Ygbuhay, R. C. 2011, AdSpR, 48, 61
Behannon, K. W., Acuña, M. H., Burlaga, L. F., et al. 1977, SSRv, 21, 235
Berdichevsky, D. B. 2009, http://vgrmag.gsfc.nasa.gov/Berdichevsky-VOY_sensor_opu090518.pdf
Berdichevsky, D. B. 2015, https://vgrmag.gsfc.nasa.gov/20151017BzPLestimates_wMAGCAL.pdf
Bridge, H. S., Belcher, J. W., Butler, R. J., et al. 1977, SSRv, 21, 259
Burlaga, L., & Ness, N. F. 2013, ApJ, 765, 35
Burlaga, L. F. 1968, SoPh, 4, 67
Burlaga, L. F. 1995, Interplanetary Magnetohydrodynamics (New York: Oxford Univ. Press)
Burlaga, L. F., McDonald, F. B., Goldstein, M. L., & Lazarus, A. J. 1985, JGR, 90, 12027
Burlaga, L. F., McDonald, F. B., & Ness, N. F. 1993, JGR, 98, 1
Burlaga, L. F., & Ness, N. F. 1968, CaJPh, 46, 1962
Burlaga, L. F., & Ness, N. F. 1994, JGR, 99, 19341
Burlaga, L. F., Ness, N. F., & Acuña, M. H. 2006, ApJ, 642, 584
Burlaga, L. F., Ness, N. F., Acuña, M. H., et al. 2008, Natur, 454, 75
Burlaga, L. F., Ness, N. F., & Richardson, J. D. 2014, JGRA, 119, 6062
Burlaga, L. F., Ness, N. F., Richardson, J. D., Decker, R. B., & Krimigis, S. M. 2016, ApJ, 818, 147
Burlaga, L. F., Ness, N. F., Wang, C., et al. 2005, ApJ, 618, 1074
Burlaga, L. F., Ness, N. F., Wang, Y.-M., & Sheeley, N. R., Jr 2009, JGR, 114, A06106
Burlaga, L. F., Ness, N. F., Wang, Y.-M., Sheeley, N. R., Jr, & Richardson, J. D. 2010, JGR, 114, A06106
Burlaga, L. F., Viñas, A. F., & Wang, C. 2007, JGR, 112, 7206
Decker, R. B., Krimigis, S. M., Roelof, E. C., et al. 2008, Natur, 454, 67
Drake, J. F., Opher, M., Swisdak, M., & Chamoun, J. N. 2010, ApJ, 709, 963
Drake, J. F., Swisdak, M., Opher, M., & Richardson, J. D. 2017, ApJ, 837, 159
Dungey, J. 1961, PhRvL, 6, 47
Gosling, J. T. 2012, SSRv, 172, 187
Gurnett, D. A., & Kurth, W. S. 2008, Natur, 454, 78
Gurnett, D. A., Kurth, W. S., Burlaga, L. F., & Ness, N. F. 2013, Sci, 341, 1489
Gurnett, D. A., Stone, E. C., Kurth, W. S., et al. 2015, ApJ, 809, 121
Krimigis, S. M., Mitchell, D. G., Roelof, E. C., & Decker, R. B. 2010, in AIP Conf. Proc. 1302, 9th Annual International Astrophysics Conf. (Melville, NY: AIP), 79
Lemaire, J., & Burlaga, L. F. 1976, Ap&SS, 45, 303
McComas, D. J., Angold, N. H., Elliott, A., et al. 2013, ApJ, 779, 2
McDonald, F. B., Webber, W. R. C., & Reames, D. V. 2010, GeoRL, 37, L18101
Opher, M., Drake, J. F., Swisdak, M., et al. 2011, ApJ, 734, 71
Parker, E. N. 1958, ApJ, 128, 664
Parker, E. N. 1963, Interplanetary Dynamical Processes (New York: Wiley-Interscience)
Pogorelov, N. V., Borovikov, S. N., Zank, G. P., & Ogino, T. 2009, ApJ, 696, 1478
Pogorelov, N. V., Heerikhuisen, J., Roytershteyn, V., et al. 2017, ApJ, in press
Richardson, J. D., & Burlaga, L. F. 2013, SSRv, 176, 4217
Richardson, J. D., Burlaga, L. F., Decker, R. B., et al. 2013, ApJ, 762, L14
Richardson, J. D., Burlaga, L. F., Drake, J. F., Hill, M. E., & Opher, M. 2016, ApJ, 831, 115
Richardson, J. D., Kasper, J. C., Wang, C., Belcher, J. W., & Lazarus, A. J. 2008, Natur, 454, 63
Richardson, J. D., Wang, C., Liu, Y. D., et al. 2017, ApJ, 834, 190
Shultz, M. 1973, Ap&SS, 34, 371
Stone, E. C., Cummings, A. C., McDonald, F. B., et al. 2008, Natur, 454, 71
Tsallis, C. 1988, JSP, 52, 479
Tsallis, C. 2009, Introduction to Nonextensive Statistical Mechanics (New York: Springer)
Washimi, H., Zank, G. P., Hu, Q., et al. 2011, MNRAS, 416, 1475
Whang, Y. C., & Burlaga, L. F. 1994, JGR, 99, 21457
Wilcox, J. N., & Ness, N. F. 1965, JGR, 70, 5793